Nanotechnology

PAPER

Uniform field electrospinning for 3D printing of fibrous configurations as strain sensors

IOP Publishing Nanotechnology
Nanotechnology 30 (2019) 375301 (9pp) https://doi.org/10.1088/1361-6528/ab29ac

Uniform field electrospinning for 3D printing of fibrous configurations as strain sensors

Qingjie Liu[1], Qiang Wu[1], Songzhi Xie, Long Zhao, Zhoujiang Chen, Zhenghua Ding and Xiaohong Li[2]

Key Laboratory of Advanced Technologies of Materials, Ministry of Education, School of Materials Science and Engineering, Southwest Jiaotong University, Chengdu 610031, People's Republic of China

E-mail: xhli@swjtu.edu.cn

Received 12 February 2019, revised 28 May 2019
Accepted for publication 13 June 2019
Published 1 July 2019

Abstract

Electrospinning is becoming an efficient method to produce fibers in the submicron range, but the bending instability of conventional electrospinning system (CES) brings limitations in the distinctive deposition of electrospun fibers. Herein, we proposed a strategy to update the electrospinning system through establishment of a uniform electric field, realizing 3D printing of electrospun fibers with well-controlled, low-cost, and template-free manners. The uniform field electrospinning (UFES) apparatus is configured by inserting the electrospinning nozzle into the center of an aided metal plate. The electric field simulation of UFES indicates a uniform distribution between the aided metal plate and the collector, while a diverging and weaker electric field is produced by CES. The collector of UFES is mounted on a translation stage, which moves along x and y axes under computer control. The distinctive deposition of electrospun fibers produces fibrous mats with rectangular patterns of different grid sizes, and butterfly and TaiJi figures with high resolutions are directly written by UFES. The layer-by-layer deposition of electrospun fibers under UFES produces microscale Mongolian yurts with distinct hollow structure. Fibrous blocks with an average width of 120 μm and height of 630 μm were printed by UFES from conductive polymer composites and constructed into strain sensors. The electric current strength of fibrous microblocks changes sharply in response to the finger bending and release, indicating the capability to monitor human motions. Thus, this study demonstrates that the UFES becomes an easy-handling strategy for 3D printing of electrospun fibers to create complex geometries.

Keywords: uniform field electrospinning, electric field simulation, distinctive fiber deposition, 3D printing, strain sensor

(Some figures may appear in colour only in the online journal)

1. Introduction

Electrospinning has gained much attention in the last decade due to its consistency in producing fibers in the submicron range. Polymers with attractive physical, chemical, mechanical, and electrical properties have been electrospun into ultrafine fibers with high hydrophobicity, chemical responsiveness, tensile strength and conductivity [1]. Owing to the superior advantages of small size, tremendous flexibility, and high surface-to-weight ratio, electrospun fibers have been applied in many fields, such as drug carriers, tissue engineering scaffolds, flexible electronics, and filters [2]. During the electrospinning process, polymer solutions or melts are charged under the action of an electric field and the electrified jet is stretched, followed by solvent evaporation and random deposition of fibers on the collector. The stretching process produces fibers with ultrafine diameters, and the interaction of the external electric field and surface charges on the jet causes the whipping instability [3, 4]. Thus, the chaotic nature of traditional electrospinning limits its applications in devices

[1] These authors contributed equally to the study.
[2] Author to whom any correspondence should be addressed.

that usually need arranged or patterned micro/nanoscale fibrous structures.

Significant progresses have been made in the construction of nanofibrous mats with different surface topographies or structural patterns by properly configuring the collectors, electrospnning system and post-treatment of fibrous mats [5]. One of the strategies to fabricate aligned and patterned fibrous mats is the collector design or post-processing treatment. Highly aligned electrospun fibers are obtained by using rotating drums, mandrels, and disks which may have different collecting geometries and various edge morphologies [6, 7]. Template conductive collectors are usually used to collect patterned fibrous scaffolds with distinct ridge/groove areas, arrayed microwells, and controllable structural cues on the surface [8, 9]. In addition, fibrous scaffolds with well-defined hole patterns are fabricated by post-treatment of randomly deposited electrospun mats via femtosecond laser ablation or solvent dissolution [10, 11]. It should be noted that the collector design is not enough to achieve distinctive deposition of electrospun fibers, and fibrous products with arbitrary hollow structures could not be fabricated through technologies mentioned above.

Another strategy is to shorten the nozzle-to-collector distance, realizing near-field electrospinning (NFES) under a low voltage. The trick of NFES technique is associated with the nearly straight line movement of polymer droplets in the initial stage of electrospinning. Thus, the bending instability can be significantly restricted to achieve the position-controlled deposition of pre-designed trajectory and the construction of aligned fibers and patterned fibrous structures [12, 13]. Brown *et al* fabricated a boxlike fibrous macrostructure by NFES through interweaving and fusion between the fiber layers [14]. By controlling the collector movement, the printed features were oriented along with the moving direction, which made it possible to print user-specific patterns [15]. However, the shortened distance between the nozzle and collector within several millimeters not only increases the risk of electric breakdown in NFES, but also limits the stretching and thinning of fibers, which tends to increase the fiber diameter. In addition, except complicated apparatus of NFES, the solvents could not be timely removed, leading to unexpected destroy of fibrous morphologies by droplets [16].

Layer-by-layer deposition of materials, better known as three-dimensional (3D) printing or additive manufacturing, has been flourishing as a fabrication process in the past several years to create complex geometries [17]. Various 3D printing technologies have been investigated such as material extrusion, binder jetting, direct energy deposition, and powder bed fusion [18]. But up to now 3D printing of fibrous scaffolds have not been realized via traditional electrospinning system. In the current study, we proposed another strategy to update the electrospinning system through establishment of a uniform electric field, realizing 3D printing of electrospun fibers with well-controlled, low-cost, and template-free manners. Figure 1(a) shows the schematic diagram of the uniform field electrospinning (UFES) apparatus. In the traditional far-field electrospinning system, an aided plate was placed close to the nozzle, and this plate-to-collector structure is supposed to generate a uniform electric field, which manipulates the motion of polymer solution jets and achieves a precise deposition of fibers on the collector. Then the nozzle or collector is modulated by the designed motion path to construct 2D or 3D fibrous scaffolds, including hollow structures as desired. In addition, 3D printed fibrous strips are investigated as potential stretchable substrates for strain sensing.

2. Materials and methods

2.1. Materials

Poly(ethylene oxide) (PEO) (M_W: 100 kDa) and polyvinylidene fluoride (PVDF) (M_W: 275 kDa) were supplied from Aladdin Regents Co., Ltd (Shanghai, China). Multiwalled carbon nanotubes (CNTs, 10–20 nm in diameter, 10–20 μm length), produced by catalytic decomposition of natural gas and purified by a concentrated acid/sonication procedure, were received from Chengdu Institute of Organic Chemistry, Chinese Academy of Sciences (Chengdu, China). All other chemicals and solvents were of reagent grade or better, and from Chengdu Kelong Reagent Co. (Chengdu, China) unless otherwise indicated.

2.2. Electrospinning

Figure 1(a) depicts the setup of UFES apparatus, containing two metal plates (aided plate and collector plate) with a distance of 40 mm. A 30-gauge stainless steel needle (inner diameter: 0.18 mm; outer diameter: 0.36 mm) was inserted into the center of the aided metal plate ($100 \times 100\,mm^2$) (figure 1(b)). The needle top was connected to the positive electrode of a high voltage station, while the cathode was connected with another metal plate ($200 \times 200\,mm^2$) as the collector. The collector was mounted on a translation stage, which moved along x and y axes under computer control. PEO solution was prepared by dissolving PEO into the mixture of distilled water and ethyl alcohol with a volume ratio of 7/3 at a concentration of 4% (w/v). PVDF solution (30%, w/v) was prepared by dissolving PVDF in the mixture of acetone and dimethylformamide at a volume ratio of 1/1, followed by blending with 5% of CNTs (w/v) under ultrasonication [19]. Polymer solutions or suspensions were added in a syringe and pumped at $1.0\,ml\,h^{-1}$ (Zhejiang University Medical Instrument Company, Hangzhou, China) to maintain a steady flow from needle. The UFES was performed under a fixed electric field using a high voltage statitron (Tianjing High Voltage Power Supply Co., Tianjing, China). As control, the conventional electrospinning system (CES) was operated with only a nozzle and a collector plate (figure 1(c)). The fiber collections were vacuum-dried to completely remove any solvent residue prior to further use.

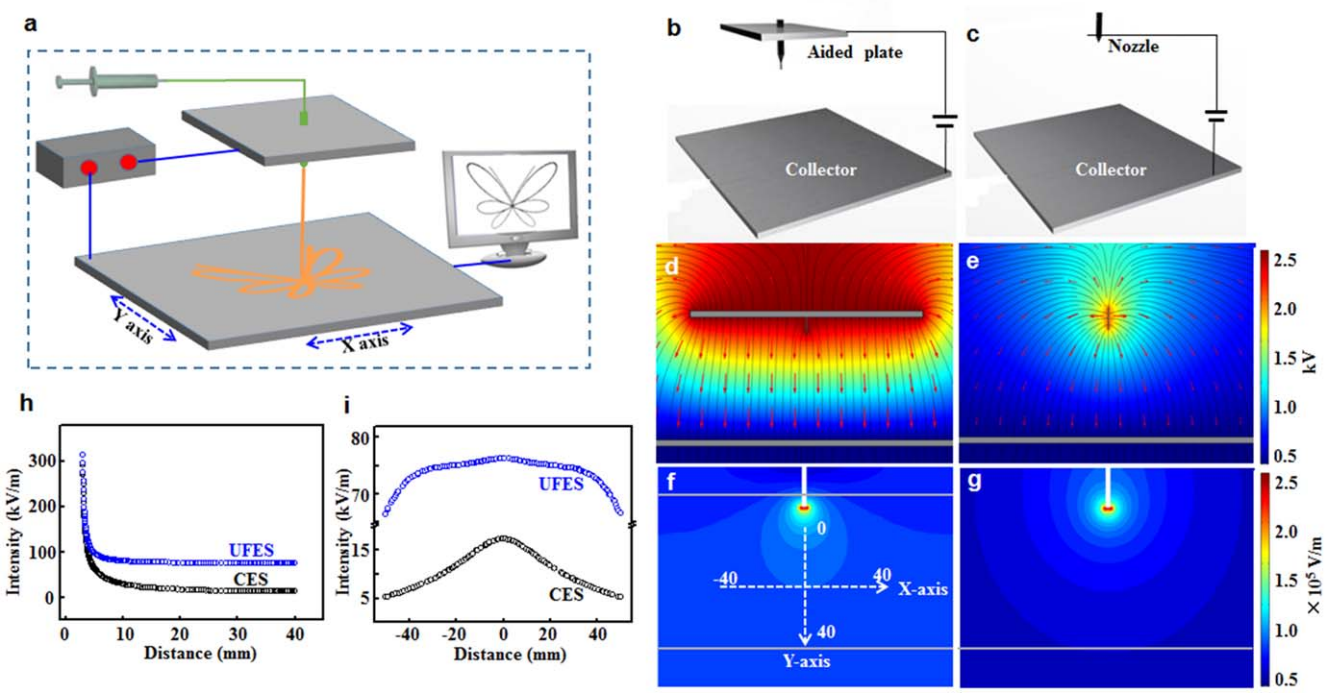

Figure 1. (a) Schematic diagram of the UFES system. (b) Schematic diagram of the UFES and (c) CES apparatus. (d) The electric field simulation of UFES and (e) CES by COMSOL. (f) The electric field intensity simulation of UFES and (g) CES by COMSOL. (h) The electric field intensity distributions from the droplet apex (0 mm) to the grounded collector (40 mm) and (i) along a line located at 20 mm above the collector.

2.3. Characterization of fibrous configurations

The fibrous morphology was determined by a scanning electron microscope (SEM, FEI Quanta 200, The Netherlands) equipped with a field-emission gun and Robinson detector after being vacuum-coated with a thin layer of gold to minimize the charging effect. The fiber diameters were determined through randomly measuring 50 fibers using ImageJ and averaging the results based on SEM images [20]. The 3D fibrous structure was observed by 3D laser scanning microscope (Keyence VK9000, Itasca, IL), and the thickness or height of fibrous configurations was measured from the 3D images using ImageJ [21]. To observe the internal appearance, 3D fibrous configurations were cut open by an ultraviolet laser marking machine (UV-3S, Han's Laser, Shenzhen, China). In addition, Rhodamine B was added in the electrospinning solution, and the fluorescent images and internal structure of 3D fibrous configurations was observed by a confocal laser scanning microscope (CLSM, Leica TCS SP2, Germany) via layer-by-layer scanning at the excitation/emission wavelengths of 540/625 nm.

2.4. Sensor construction and testing

3D fibrous microblocks of PVDF/CNTs were deposited on a poly(urethane) (PU) membrane, which was covered on the metal collector. The collector was moved at a reciprocating manner at 0.04 m s^{-1} to obtain fibrous microblocks with different thickness after stacking 40, 80, 120, and 160 layers. Two copper wires with a distance of 6 mm were fixed on the two ends of microblocks by using silver paste as the sensor electrodes. The resistance and current of fibrous microblocks were readout directly from Keithley 6514 system electrometer under a 5 V DC power supply [22], then, the conductivity (reciprocal of resistance) and current–voltage (I–V) were obtained. The fibrous microblocks were assembled on a forefinger, and the electric current strength was recorded after cyclical bending and release actions.

3. Results and discussion

3.1. Electric field analysis of UFES

When a high voltage is applied to the electrospinning system, the pendent drop of polymer suspensions at the needle tip becomes highly electrified with an even distribution of the induced charges over the surface. There are two major types of electrostatic forces on the drop: electrostatic repulsion between the surface charges and Coulombic force exerted by the external electric field [23]. Under the action of these electrostatic forces, the liquid drop is distorted into a conical shape commonly known as the Taylor cone [24, 25]. Once the electric field strength surpasses a threshold, the electrostatic forces overcome the surface tension of the polymer solution and the liquid is ejected as a jet from the needle. The Coulombic force exerted by the electric field drives nanofibers moving along electric field lines, and the electric field intensity on the Taylor cone determines the electric charge density on fibers. Thus, the distribution and intensity of the

electric field play dominant roles in controlling precisely the fiber movement and deposition [26].

In the current study the finite element based software package COMSOL Multiphysics® was used to study the electric field configuration of UFES and compared with that of CES [26, 27]. To simplify the simulation, it is assumed no charge dissipation for approximation, and the dielectric coefficient is assumed as 1 [28]. Figure 1(d) shows the global electric field distribution of UFES, indicating a uniform electric field between the aided metal plate and the collector. A single spinning jet initiates from the needle tip, moves along the electric field line without whipping and deposits precisely on the collector. However, a diverging electric field between the needle and a metal collector is produced in the CES (figure 1(e)), leading to multiple and titled jet drawn from the Taylor cone at the needle tip. The electrified jet then undergoes a stretching along the diverging electric field and the whipping process results in a disorder fiber deposition on the collector. Figures 1(f) and (g) display the simulation results of electric field strength in UFES and CES, where different colors represent the gradients of electric field intensity. Compared with CES, UFES indicates less significant decreases in the electric field strength between the nozzle and collector plate. In addition, when the electrospinning voltages are set as 3 and 1.3 kV for UFES and CES, respectively, the same electric field strengths on the Taylor cone are obtained at $3.7 \times 10^5\ \mathrm{V\,m^{-1}}$ that can initiate the ejection of polymer solutions [29].

Figure 1(h) shows the corresponding electric field intensity along a line from the droplet apex (0 mm) to the grounded collector (40 mm), indicating a rapid decline of the electric field intensity in UFES and CES. The average electric field intensity of UFES between 0 and 30 mm is around $0.8 \times 10^5\ \mathrm{V\,m^{-1}}$, which is 4 folds higher than that of CES ($0.2 \times 10^5\ \mathrm{V\,m^{-1}}$). Figure 1(i) shows the distribution of electric field intensities along a line located at 20 mm above the collector. The electric field intensity of CES shows an uneven distribution and a rapid decrease at the both sides. However, UFES displays a straight line below the apex of needle, indicating an electric field with uniform distribution and high intensity around the needle apex. In addition, the polymer fluid jet can be recognized as series connected beads, thus the formula $Fe = E \times Q$ can be approximately used to describe the relations between the electrostatic force (Fe), electric field intensity (E) and charge quantity (Q) [30, 31]. The charge density is defined as the Q value per unit on the jet, which comes from corona discharge [23]. As indicated above, UFES and CES have the same electric filed intensities ($3.7 \times 10^5\ \mathrm{V\,m^{-1}}$) on the needle tips to reach the threshold for electrospinning, thus their Q values should be same. In addition, the charges stored in polymer jets contribute to the jet stretching by electrostatic forces under electric field. The higher applied voltage in UFES (4 kV) resulted in a higher electric field intensity (E) and then larger electrostatic force (Fe) than those of CES. The high Coulombic force exerted by the uniform external electric field in UFES could suppress the electrostatic repulsion of charges on the fiber surface. Therefore, a uniform and strong electric field is able to produce a single jet on Taylor cone and move along the electric field direction. Compared with that of CES, the whipping instability of fibers is significantly inhibited and higher accuracy of fiber depositions could be achieved by UFES.

3.2. Construction of 2D fibrous figures by UFES

In the current study, fibers were deposited on the collector moving along x and y axes under computer control. As shown in figure 2(a), the fiber diameters decreased as the electrospinning distance increased and reached a plateau when the distance was beyond 40 mm. Thus the distance between the collector and the aided plate was fixed at 40 mm. Figure 2(b) shows SEM images of collected fibers after deposition on collectors moving at speeds from 0.04 to $0.64\ \mathrm{m\,s^{-1}}$. The higher moving speed of collectors ($0.64\ \mathrm{m\,s^{-1}}$) led to the collection of straight fibers. With the decrease in the moving speed, waved and coiled fibers were deposited on collectors to obtain fibrous strips [15]. It should be noted that the width of fibrous mats indicated a slight increase with the decrease in the scanning speed of collectors. A fibrous strip with a higher density of fibers was obtained at the moving speed of $0.04\ \mathrm{m\,s^{-1}}$.

The collector was mounted on a 2D motion platform which was precisely controlled by computer program, so the fibers with pre-designed trajectories can be deposited. Figure 2(c) shows SEM images of fibrous meshes after deposition on collectors scanning along the vertical and horizontal directions. The space between the line trajectories varied from 100 to 400 μm, and well-arranged fibrous mats were obtained with rectangular patterns of different grid sizes. As shown in the magnified images (figure 2(d)), fibers were spirally deposited on the ridge of patterns and the average fiber diameter was around 150 nm.

Except the direct lines, the collector moved in a curved path and fibers were collected with different configurations. Figures 2(e) and (f) shows the outlines of butterfly and TaiJi figures, which were input in computers to design the moving profiles of collectors. Figure 2(g) and h show SEM images of butterfly and TaiJi figures, consisting of smooth fibrous lines. All the images were less than 1 $\mathrm{mm^2}$ in size with a line width of less than 100 μm. Kim *et al* modified the electrospinning process with a cylindrical auxiliary electrode to stabilize the initially electrospun jets; The width of the obtained fibrous mat was about 10 mm even after collecting under an alternating-current electric field generated by a parallel-plate electrode [32]. Wu *et al* employed an auxiliary electrode positioned directly behind a rotating collector to direct the fiber orientation; the width of the final mats generated was over 2 cm even after the addition of two additional auxiliary electrodes to assist in converging the electric field [33]. Therefore, it was indicated that UFES could directly write patterned fibrous mats with high resolutions.

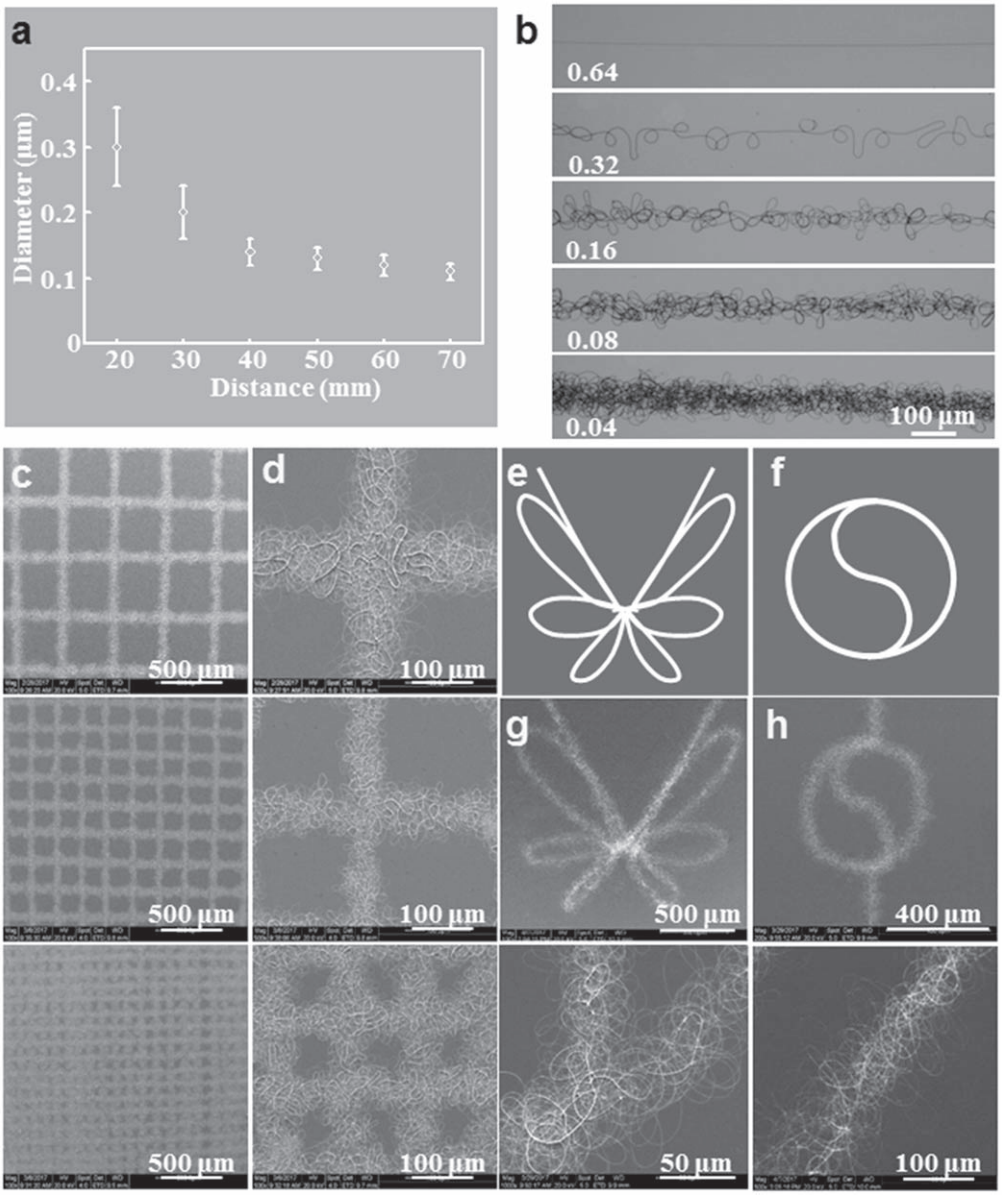

Figure 2. (a) Fiber diameters as a function of electrospinning distance in UFES. (b) SEM images of collected fibers after UFES deposition on collectors moving at speeds from 0.04 to 0.64 m s^{-1}. (c) SEM images and (d) magnified images of fibrous mats after deposition on collectors scanning along the vertical and horizontal directions. (e) Outlines of butterfly and (f) TaiJi figures which are input in computers to design the moving profiles of collectors. (g) SEM images and magnified images of butterfly and (h) TaiJi figures after UFES deposition.

3.3. 3D printing of fibrous configurations by UFES

To print 3D fibrous configurations, the collector was moved in a circle track and fibers were deposited layer-by-layer. Figure 3(a) shows the 3D images of fibrous tubes of different heights after deposition of different layers. The height of the printed walls increased from about 160–630 μm when the printed layers increased from 40 to 160. The collector was moved in a circular manner and the diameter of the circles decreased gradually to obtain a Mongolian yurt. Figure 3(b) shows SEM images of the Mongolian yurt with a base diameter of around 900 μm and height of around 600 μm. A hollow structure of the Mongolian yurt was present after cutting into two halves (figures 3(c), (d)), and the yurt wall was composed of electrospun fibers with a diameter of around 140 nm (figure 3(e)). Figure 3(f) shows a fluorescent yurt. The layer-by-layer scanning images of the fluorescent yurt revealed distinct hollow structure (figure 3(g)). It should be noted that the structure could not be constructed by CES. Thus, the UFES system allowed the printing of microstructures with fully enclosed internal cavities at a high resolution.

3.4. Fibrous microblocks as strain sensors

Stretchable electronics have aroused attentions for potential applications including, but not limited to, deformable, foldable, rollable, and bendable displays [34, 35]. Stretchable strain sensors are essential parts of these electronics, and

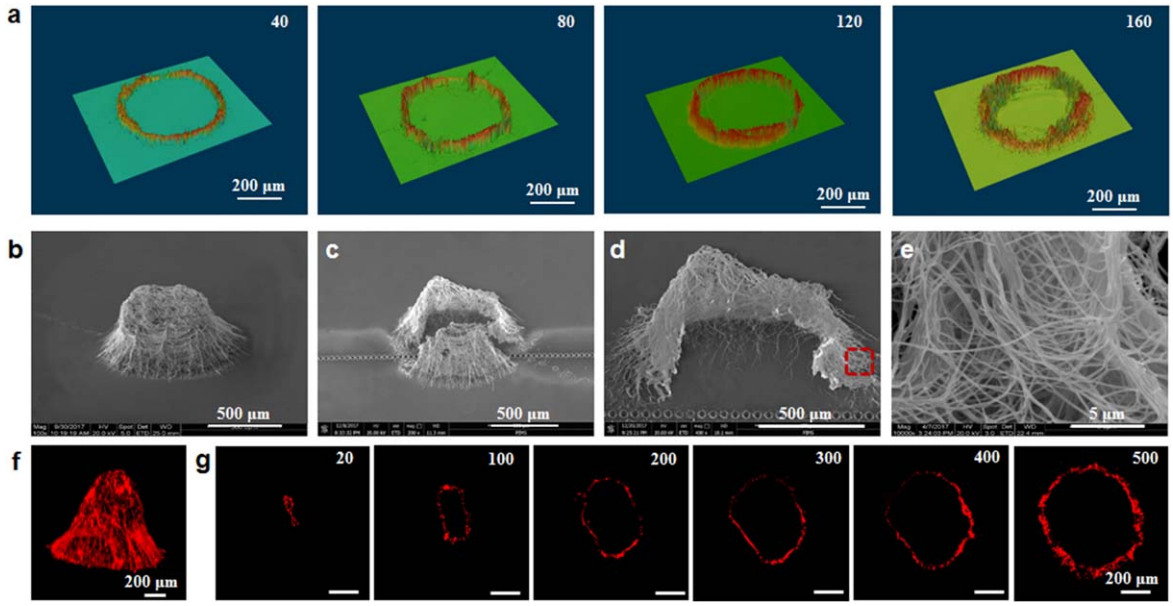

Figure 3. Construction of 3D fibrous structure. (a) 3D images of fibrous tubes of different heights after deposition of 40−160 layers. (b) SEM images of a Mongolian yurt, (c), (d) the yurt after laser cutting and (e) fibers in the yurt wall. (f) CLSM images and (g) layer-layer scanning images of the Mongolian yurt after embedding rhodamine in fibers. The numbers in the images denote the depth (μm) of CLSM scanning from the yurt top.

attempts have made to develop different fabrication methods and achieve stable performances [36, 37]. One of the most formidable challenges of the stretchable sensors is the retention of high conductivity even under severe deformation. The application of nonwoven membranes is limited by their disordered fiber positioning. Herein, fibrous microblocks made from PVDF/CNTs blends were investigated as substrates for strain sensing. Figure 4(a) shows SEM images of fibrous microblocks prepared after deposition of 40, 80, 120, and 160 layers by UFES. The 3D images showed that the height of fibrous microblocks increased from about 200–700 μm after deposition from 40 to 160 layers (figure 4(b)). The magnified images indicated that the microblocks were composed of curled fibers that joined by each other, and the average fiber size was around 350 nm (figure 4(c)).

Figure 4(d) illustrates the schematic depiction of the fabricating process of strain sensors from fibrous microblocks. It is well known that the performance of a strain sensor is characterized by a gauge factor for practical application, which is defined as $(dR/R)/(dL/L)$, where R is the resistance of the sensor, L is the distance between the electrodes on the sensor (6 mm), and dR and dL are the resistance and length changes of sensors during stretching [38]. To measure the sensitivity of the sensor to strains, the fibrous blocks were stretched at the rates (dL/L) from 0% to 320% by a custom-built computer-controlled stretching apparatus along the strip direction. Figure 4(e) shows that the resistances of sensors with different heights as a function of the tensile rates. The initial resistance of the fibrous blocks of 40 and 80 layers was larger than others, and the resistance value increased sharply with the increase in the strains. The large resistance after a tiny strain suggested that limited strains could be applied during stretching. The resistance of 160-layered blocks indicated few changes during the stretching process, resulting in a limited sensitivity as a strain sensor. The fibrous blocks of 120 layers with average width of 120 μm and height of 630 μm showed a gradual increase in the resistance to strains during stretching. It can be seen that the sensor tolerated strains up to 240%, and the sensor resistance was infinity above the strain of 240%. In addition, because the fibrous block was a 3D structure obtained by stacking multiple layers of curved fibers, fibers would not be broken when subjected to greater deformations and the strain sensor could maintain good conductivity even if subjected to large strains. Figure 4(f) shows the *I–V* characteristics of 120-layered sensors with different uniaxial strains. The electric current strengths decreased gradually with the stretching varying from 0% to 240%, but the resistance of the sensor indicated no change at the same strains. Zheng *et al* fabricated highly aligned electrospun fiber arrays of PVDF/CNTs and twisted into fibrous ropes for strain sensing. The electrical resistance was only sensitive to limited strains and fluctuations of resistances were observed in the *I–V* curves [13]. Here, the fibrous blocks with stacked curved fibers could bear strains of 240% without breaking and achieve better resistance stability under strains.

The fibrous microblock sensor could maintain high conductivity even under the strain limit, which means the potential application of the device as strain sensors [39, 40]. The conventional hospital-centered healthcare sensing devices have limitations due to the poor portability and wearability. Future strain sensors could also be incorporated into smart clothes or attached directly to the body to monitor human motion, disease diagnosis, virtual reality and health assessment [41, 42]. In the current study, the microblock sensor was assembled on a forefinger to record the electric

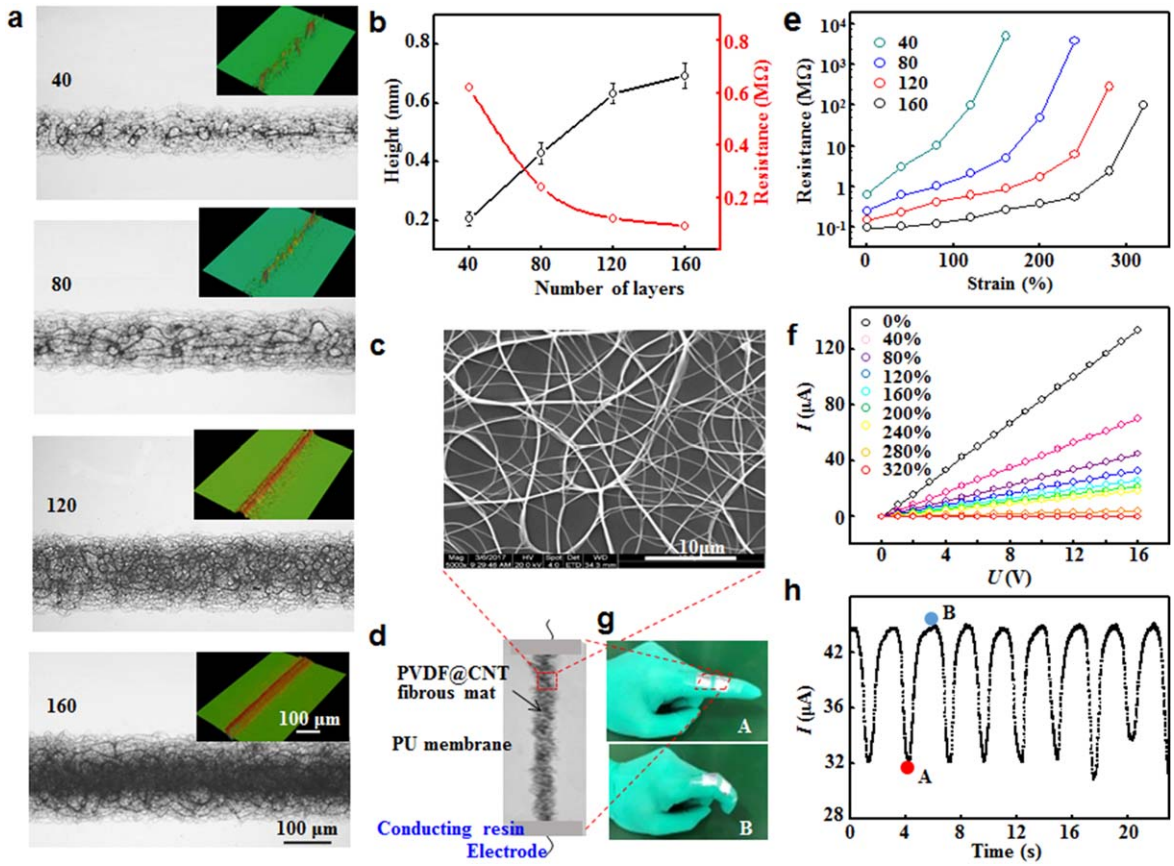

Figure 4. Fibrous microblocks as strain sensors. (a) SEM images of fibrous microblocks prepared after deposition of different layers by UFES, and the inset shows 3D images. (b) The height and the resistance of fibrous microblocks after UFES deposition of different layers. (c) SEM images of fibers in the microblocks. (d) Schematic depiction of strain sensor fabrication. (e) Resistances of strain sensors with different heights (μm) as a function of the strains. (f) *I–V* characteristics of strain sensor after UFES deposition of 120 layers under different uniaxial strains. (g) Images of forefingers assembled with fibrous sensors to record the electric current strength during the bending and release actions. (h) Electric current strength changes of the fibrous sensors after different cycles of bending and release.

current strength during the bending and release actions (figure 4(g)). Figure 4(h) summarizes the electric current strength changes of the fibrous microblocks after different cycles of bending and release. When the demonstrator's finger was suddenly bended (point A), the electric current strength decreased sharply, indicating an immediate response to the finger actions. As the angle of the bending finger was not absolutely unanimous, the current strength may differ a little at the bending point of the finger in each cycle. Furthermore, once the finger was completely unfolded, the electric current strength returned sharply to the initial value (point B). The current strength could fully recover to its original value at the unfolding point in each cycle. Thus, 3D printing of electrospun fibers have been realized by UFES with well-controlled, low-cost, and template-free manners, and the 3D printed fibrous microblocks are capable of monitoring human motions, indicating potentials as parts of robots and in human-machine interfacing applications. Recently Qu *et al* demonstrated a novel strategy to fabricate superelastic fibers from multiple materials by thermal drawing. Such fibers possess the unique ability to simultaneously detect the location, direction and amplitude of strains [43]. Attempts should be made to optimize the component, size and arrangement of 3D printed fibers to expand the sensing performance.

4. Conclusions

In the current study the UFES is developed to realize distinctive deposition of electrospun fibers and 3D printing of complex structures. The UFES apparatus is configured by inserting the electrospinning nozzle into the center of an aided metal plate. The electric field simulation of UFES indicates a uniform distribution between the aided metal plate and the collector. Except fibrous mats with rectangular patterns of different grid sizes, butterfly and TaiJi figures are obtained by 2D printing of electrospun fibers, and 3D printing via UFES produces microscale Mongolian yurts with distinct hollow structure. 3D printed fibrous microblocks form conductive polymer composites are constructed into strain sensors, and the currents change sharply in response to the finger bending and release, indicating the capability to monitor human motions. Thus, this study demonstrates a well-controlled and easy-handling strategy of UFES for 3D printing of electrospun fibers.

Acknowledgments

This work was supported by National Natural Science Foundation of China (31771034 and 31470922), Key Research and Development Program of Sichuan Province (2018SZ0348), Cultivation Program for the Excellent Doctoral Dissertation of Southwest Jiaotong University and the Analytical and Testing Center of Southwest Jiaotong University for SEM analysis.

ORCID iDs

Xiaohong Li https://orcid.org/0000-0003-1312-0215

References

[1] Nasajpour A, Mandla S, Shree S, Mostafavi E, Sharifi R, Khalilpour A, Saghazadeh S, Hassan S, Mitchell M J and Leijten J 2017 Nanostructured fibrous membranes with rose spike-like architecture *Nano Lett.* **17** 6235–40

[2] Walser J, Stok K S, Caversaccio M D and Ferguson S 2016 Direct electrospinning of 3D auricle-shaped scaffolds for tissue engineering applications *Biofabrication* **8** 025007

[3] Andreas G and Wendorff J H 2007 Electrospinning: a fascinating method for the preparation of ultrathin fibers *Angew. Chem., Int. Ed.* **46** 5670–703

[4] Cheng J, Jun Y, Qin J and Lee S H 2017 Electrospinning versus microfluidic spinning of functional fibers for biomedical applications *Biomaterials* **114** 121–43

[5] Xue J J, Wu T, Dai Y Q and Xia Y N 2019 Electrospinning and electrospun nanofibers: methods, materials, and applications *Chem. Rev.* **8** 5298–415

[6] Dong Y, Ding Y, Duan Y, Su J, Yin Z and Yong A H 2018 Large-scale direct-writing of aligned nanofibers for flexible electronics *Small* **14** 1703521

[7] Persano L, Dagdeviren C, Su Y, Zhang Y, Girardo S, Pisignano D, Huang Y and Rogers J A 2016 High performance piezoelectric devices based on aligned arrays of nanofibers of poly(vinylidenefluoride-co-trifluoroethylene) *Nat. Commun.* **4** 1633

[8] Zhao S, Zhou Q, Long Y Z, Sun G H and Zhang Y 2013 Nanofibrous patterns by direct electrospinning of nanofibers onto topographically structured non-conductive substrates *Nanoscale* **5** 4993–5000

[9] Yu G F, Yan X, Yu M, Jia M Y, Pan W, He X X, Han W P, Zhang Z M, Yu L M and Long Y Z 2016 Patterned, highly stretchable and conductive nanofibrous PANI/PVDF strain sensors based on electrospinning and *in situ* polymerization *Nanoscale* **8** 2944–50

[10] Sun B, Long Y Z, Zhang H D, Li M M, Duvail J L, Jiang X Y and Yin H L 2014 Advances in three-dimensional nanofibrous macrostructures via electrospinning *Prog. Polym. Sci.* **39** 862–90

[11] Jia C, Yu D, Lamarre M, Leopold P L, Teng Y D and Wang H 2014 Patterned electrospun nanofiber matrices via localized dissolution: potential for guided tissue formation *Adv. Mater.* **26** 8192–7

[12] He X X, Zheng J, Yu G F, You M H, Yu M, Ning X and Long Y Z 2017 Near-field electrospinning: progress and applications *J. Phys. Chem.* C **121** 8663–78

[13] Zheng J, Xu Y, Li M M, Yu G F, Zhang H D, Wojciech P, He X X, Jean-Luc D and Long Y Z 2015 Electrospun aligned fibrous arrays and twisted ropes: fabrication, mechanical and electrical properties, and application in strain sensors *Nanoscale Res. Lett.* **10** 475

[14] Brown T D, Dalton P D and Hutmacher D W 2011 Direct writing by way of melt electrospinning *Adv. Mater.* **23** 5651–7

[15] Zhang B, He J, Li X, Xu F and Li D 2016 Micro/nanoscale electrohydrodynamic printing: from 2D to 3D *Nanoscale* **8** 15376–88

[16] Chang C, Limkrailassiri K and Lin L 2008 Continuous near-field electrospinning for large area deposition of orderly nanofiber patterns *Appl. Phys. Lett.* **93** 123111

[17] Murphy S V and Atala A 2014 3D bioprinting of tissues and organs *Nat. Biotechnol.* **32** 773–85

[18] Ligon S C, Liska R, Stampfl J, Gurr M and Mülhaupt R 2017 Polymers for 3D printing and customized additive manufacturing *Chem. Rev.* **117** 10212–90

[19] Liu Y, Lu J, Xu G, Wei J, Zhang Z and Li X 2016 Tuning the conductivity and inner structure of electrospun fibers to promote cardiomyocyte elongation and synchronous beating *Mater. Sci. Eng.* C **69** 865–74

[20] Wang J, Chen N, Ramakrishna S, Tian L L and Mo X M 2017 The Effect of plasma treated PLGA/MWCNTs-COOH composite nanofibers on nerve cell behavior *Polymers* **9** 713

[21] Yin C, Jatoi A W, Bang B, Gopiraman M and Kim I S 2016 Fabrication of silk fibroin based three dimensional scaffolds for tissue engineering *Fibers Polym.* **17** 1140–5

[22] Zhang L *et al* 2016 Lawn structured triboelectric nanogenerators for scavenging sweeping wind energy on rooftops *Adv. Mater.* **28** 1650–6

[23] Collins G, Federici J, Imura Y and Catalani L H 2012 Charge generation, charge transport, and residual charge in the electrospinning of polymers: a review of issues and complications *J. Appl. Phys.* **111** 044701

[24] Salehhudin H S, Mohamad E N, Wan N L M and Afifi A M 2017 Multiple-jet electrospinning methods for nanofiber processing: a review *Mater. Manuf. Process.* **33** 479–98

[25] Taylor G 1966 Studies in electrohydrodynamics: I. The circulation produced in a drop by electrical field *Proc. R. Soc.* A **291** 159–66

[26] Savva I, Evaggelou E, Papaparaskeva G, Leontiou T, Stylianopoulos T, Mpekris F, Stylianou K and Krasiachristoforou T 2015 Alignment of electrospun polymer fibers using a concave collector *RSC Adv.* **5** 104400–7

[27] Wang X, Wang X and Lin T 2012 Electric field analysis of spinneret design for needleless electrospinning of nanofibers *J. Mater. Res.* **27** 3013–9

[28] Lauricella M, Melchionna S, Montessori A, Pisignano D, Pontrelli G and Succi S 2018 Entropic lattice Boltzmann model for charged leaky dielectric multiphase fluids in electrified jets *Phys. Rev.* E **97** 033308

[29] Reneker D H and Chun I 1999 Nanometre diameter fibres of polymer, produced by electrospinning *Nanotechnology* **7** 216–23

[30] Reneker D H, Yarin A L, Fong H and Koombhongse S 2000 Bending instability of electrically charged liquid jets of polymer solutions in electrospinning *J. Appl. Phys.* **9** 4531–47

[31] Li K L, Xu Y L, Liu Y, Mohideen M M, He H F and Ramakrishna S 2019 Dissipative particle dynamics simulations of centrifugal melt electrospinning *J. Mater. Sci.* **54** 9958–68

[32] Kim G H 2010 Electrospinning process using field-controllable electrodes *J. Polym. Sci. Polym. Phys.* **44** 1426–33

[33] Wu Y L, Carnell A and Clark R L 2007 Control of electrospun mat width through the use of parallel auxiliary electrodes *Polymer* **48** 5653–61

[34] Pan X, Wang Z, Cao Z, Zhang S, He Y, Zhang Y, Chen K, Hu Y and Gu H 2016 A self-powered vibration sensor based on electrospun poly(vinylidene fluoride) nanofibres with enhanced piezoelectric response *Smart Mater. Struct.* **25** 105010

[35] Yan C Y, Kang W B, Wang J X, Cui M Q, Wang X, Foo C Y, Chee K J and Lee P S 2014 Stretchable and wearable electrochromic devices *ACS Nano* **8** 316–22
[36] Amjadi M, Kyung K U, Park I and Sitti M 2016 Stretchable, skin-mountable, and wearable strain sensors and their potential applications: a review *Adv. Funct. Mater.* **26** 1678–98
[37] Yan W, Page A, Dang T N, Qu Y P, Sordo F, Wei L and Sorin F 2019 Advanced multimaterial electronic and optoelectronic fibers and textiles *Adv. Mater.* **31** 1802348
[38] Gong S, Schwalb W, Wang Y, Chen Y, Tang Y, Si J, Shirinzadeh B and Cheng W 2014 A wearable and highly sensitive pressure sensor with ultrathin gold nanowires *Nat. Commun.* **5** 4132
[39] Park M, Im J, Shin M, Min Y, Park J, Cho H, Park S, Shim M B, Jeon S and Chung D Y 2012 Highly stretchable electric circuits from a composite material of silver nanoparticles and elastomeric fibres *Nat. Nanotechnol.* **7** 803–9
[40] Cheng Y, Wang R, Sun J and Gao L 2015 Highly conductive and ultra-stretchable electric circuits from covered yarns and silver nanowires *ACS Nano* **9** 3887–95
[41] Chortos A, Liu J and Bao Z 2016 Pursuing prosthetic electronic skin *Nat. Mater.* **15** 937–50
[42] Ko H, Lee J, Kim Y, Lee B, Jung C H, Choi J H, Kwon O S and Shin K 2014 Active digital microfluidic paper chips with inkjet-printed patterned electrodes *Adv. Mater.* **26** 2335–40
[43] Qu Y P, Dang T N, page A G, Yan W, Gupta T D, Rotaru G M, Rossi R M, Favrod V D, Bartolomei N and Sorin F 2018 Superelastic multimaterial electronic and photonic fibers and devices via thermal drawing *Adv. Mater.* **30** 1707251